Materials and Structures (2020) 53:103
https://doi.org/10.1617/s11527-020-01536-2

ORIGINAL ARTICLE

Experimental pull-out tests and design indications for strength anchors installed in masonry walls

Linda Giresini · Mario Lucio Puppio · Francesca Taddei

Received: 14 January 2020 / Accepted: 14 July 2020 / Published online: 24 July 2020

Abstract This study deals with the identification of the mechanical behavior of chemical anchors embedded in masonry walls. 108 pull-out tests are carried out in five types of masonry walls built with clay brick or vertically perforated units with cement mortar. Different parameters are taken into account: embedment depths, masonry type, anchor position (injection either in brick units or in mortar joints). The axial load capacity and the failure mode are observed for each test. The results are examined by means of elastic and plastic models assessing the efficiency of anchors installed in headers, stretchers or mortar joints. The anchors injected in mortar joints are shown to have much greater pull-out capacity than that found for anchors in bricks. Passing from 90 to 160 mm of embedment depth, a minimum increase by 40% of pull-out strength is observed. The most common failure modes are the sliding failure, which occurs for short anchors or weak masonry, and mixed sliding/cone failure, for long anchors or strong masonry. An analytical model is proposed to design anchors in order to avoid or at least to limit brittle masonry failures and to identify the field of application of uniform stress models.

Keywords Pull-out · Chemical anchors · Epoxy resin injection · Masonry · Pull-out capacity · Embedment depth · Sliding failure

L. Giresini (✉) · M. L. Puppio
Department of Energy Systems, Territory and Constructions Engineering, University of Pisa, Largo Lucio Lazzarino 1, 56100 Pisa, Italy
e-mail: linda.giresini@unipi.it

M. L. Puppio
e-mail: mariolucio.puppio@unipi.it

F. Taddei
Lehrstuhl für Baumechanik, Technical University of Munich, Munich, Germany
e-mail: francesca.taddei@tum.de

Abbreviations

E	Steel young modulus
f'	Masonry compressive strength
f'_{EC6}	Masonry compressive strength as in EC6
f_y	Anchor tensile strength
G_{er}	Shear modulus of the epoxy resin
G_m	Shear modulus of masonry
h	Embedment depth
h_c	Cone depth
h_{ef}	Depth epoxy resin
h_{max}	Maximum embedment depth
K	Stiffness of the bond spring per unit length
k	Stiffness of the bond springs per unit bond surface and unit slip
P	Applied tensile force
P_{max}	Pull-out strength
P_s	Resistance of the threaded anchor
r_m	Radius of the masonry cylinder

r_s	Radius of the steel bar
$t_a = (\phi_0 - \phi)/2$	Thickness of the adhesive layer
$\eta_s = P_{max}/P_s$	Efficiency of the anchors
λ'	Coefficient related to the characteristic of the resin and of the epoxy bar
$\lambda = E_s A_s / E_m A_m$	Relative axial stiffness of the steel bars versus the material support
λ_w	Slenderness ratio of the walls (height/thickness)
Σ	Adherent perimeter
τ_0	Masonry shear stress
τ_{0EC6}	Masonry shear strength as in EC6
τ_{0m}	Masonry shear stress from analytical models
τ_c	Mean uniform bond stress
τ_m	Shear stress of the cylinder m
τ_{max}	Max shear stress of the masonry
τ_s	Shear stress of the steel bar
$\tau(z)$	Shear stress along the z direction
ϕ	Nominal diameter of the anchors
ϕ_0	Nominal diameter of the hole
t_{min}	Minimum thickness of the walls
t	Thickness of the walls

1 Introduction

Strength anchors are extensively used in repairing and retrofitting existing structures with low resistance [1–6] and to secure endpoints of lifelines. When dynamic actions are involved, especially close to rocking resonance conditions [7, 8], their pull-out strength plays a crucial role, e.g. in connections between masonry walls and timber diaphragms or roofs [9–12].

In case of chemical anchors, the adhesive component of the system is generally resin, in particular vinyl resin with polyester, polyester with or without styrene, or two epoxy components. Currently, two European standards cover the topic: the European Technical Approval Guidelines (ETAG) for chemical anchors in concrete [13] and the ETAG for chemical anchors in masonry [14].

As for anchors embedded in concrete, numerous experimental data are available to assess the influence of boundary conditions and of base material on the anchors strength. Over one thousand tests on chemical anchors combined with twenty resin types showed that the parameters that mostly influenced the mechanical behavior were compressive strength and cracking of concrete, hole cleanliness and humidity, high temperatures and curing time [15–17]. These studies highlighted that, increasing concrete compressive strength, anchor diameter and embedment depth, the anchor tensile capacity increases. More recent experimental tests confirmed these results [2]. Moreover, the axial capacity was observed to be highly sensitive to the cleansing of the drilled hole: water cleansing gave better results than air cleansing, while no cleaned holes resulted in a strong decrement of the anchor pull-out capacity [2]. Since the experimental tests are often expensive and long lasting, smart evaluation systems like artificial neural networks can be used to determine the anchoring performance in concrete [18, 19].

As for anchors embedded in masonry, the behavior of adhesive anchors highly depends on masonry texture and quality [20, 21]. In particular, the heterogeneity of historic masonry causes a remarkable dispersion of the local resistance of masonry and therefore of the anchor itself [4]. The response may show wide scatter depending on whether the masonry is rubble or composed by traditional [22, 23] or bio components [24]. However, in the past, steel tie rods were widely used to strengthen any type of historical masonry construction against seismic and other dynamic actions, especially in the out-of-plane failure modes [25–27]. Nowadays, chemical anchors are extensively used in the seismic retrofitting of existing masonry buildings [28], especially in case of structural irregularity which could cause a greater vulnerability [29, 30]. Structural anchors are also used in thermal retrofitting [31, 32] for the application of external coating.

As a consequence, contrary to anchors embedded in concrete, many uncertainties arise for a reliable estimation of pull-out capacity in case of diverse wall types and embedment depths different from those standardized. Moreover, the anchor capacity strongly depends on the anchor material, which can be the traditional steel or the more innovative Fiber Reinforced Plastic (FRP) (with durability advantages) [33, 34]. An extensive review of design formulations for injected anchors and experimental tests in masonry elements can be found in [33]. In this work, the main parameters influencing the pull-out capacity and the

failure modes were found to be the embedment length and the anchor diameter. On the other hand, not clear trends were evidenced about the effects of the mechanical properties of masonry and injection grout [33].

As for the available standards of anchors in masonry [14] (Annex C), some design methods are specified and four failure modes are identified: (1) steel failure, (2) anchor pull-out failure, (3) brick breakout failure and (4) pull-out of one brick. The influence of joints is also taken into account in the proofs of the anchor. With the exception of mode (1), the other failure modes are strictly dependent on the nature of the base material (masonry), on the type of epoxy resin, on the embedment depth and on their combination.

Unfortunately, little information is available when dealing whit anchors installed in mortar joints, situation not always unavoidable. Indeed, this case often occurs when anti-fall devices are installed into plastered masonry walls. Arifpovic and Nielsen provided analytical expressions for obtaining the pull-out capacity of anchors in mortar joints [21].

When experimental tests are not available, analytical models or numerical simulations can be used to assess the strength of chemical anchors. The former can be based on the plasticity theory [35–37] and on the elasticity theory [38, 39], but generally refer to anchors embedded in concrete [40]. Numerical simulations with finite element models can predict the pull-out capacity of anchors and the progression of damage considering concrete [41] or masonry [42] as base material. All these approaches are finalized to correctly estimate the pull-out capacity of strength anchors, providing design recommendations [33, 43, 44]. The present paper intends to follow this direction, broadening the knowledge of the behavior of strength anchors in masonry specimens, by interpreting the results of 108 pull-out tests. These tests are performed on chemical anchors with three embedment depths and in five masonry walls of clay brick (solid and vertically perforated) and autoclaved and aerated concrete.

Section 2 contains a description of the experimental campaign including results and their elaboration, whereas Sect. 3 analyzes the analytical models for the interpretation of the experimental tests and design indications for strength anchors in masonry walls.

2 Experimental campaign

The experimental campaign consisted in performing 108 pull-out tests on chemical anchors injected with three embedment depths (90, 120 and 160 mm) in both units (stretchers and headers) and mortar joints.

2.1 Description of the specimens

Five masonry walls were built in an open-air laboratory adopting different types of base material and geometric configurations on a C30/35 r.c. foundation beam wall thickness 25, 30 and 36 cm (Figs. 1, 2):

A. Clay brick (dimensions $24 \times 12 \times 5.5$ cm^3)—wall thickness 36 cm
B. Clay brick ($24 \times 12 \times 5.5$ cm^3)—wall thickness 25 cm
C. Autoclaved aerated concrete AAC ($25 \times 30 \times 18.5$ cm^3)—wall thickness 25 cm
D. Vertically perforated units ($25 \times 30 \times 18.5$ cm^3), percentage of voids $<$ 36%—wall thickness 30 cm
E. Vertically perforated units ($25 \times 30 \times 18.5$ cm^3), percentage of voids $<$ 36%—wall thickness 25 cm

For all the specimens, cement-based mortar was used: autoclaved aerated concrete (AAC) units were coupled with M10 mortar (nominal compressive strength 10 MPa), whereas clay bricks were combined with M5 mortar (nominal compressive strength 5 MPa). In order to confirm the mechanical parameters declared by the manufacturer, PNT-G tests [45] and laboratory compression and bending tests were performed. In particular, the former is an indirect non-destructive method to in situ assess the mortar compressive strength, based on the measurement of the amount of energy required to drill a 5 mm cavity in the joint. For compression strengths lower than 4 MPa, typical of many historical buildings, the drilling work does not depend on the aggregate type and therefore, in this case, the influence of grain size distribution can be neglected. For each wall, 15 measures were performed considering them acceptable when the difference between at least five of the values was less than 25% of the mean. The mean values of compression strength obtained following this

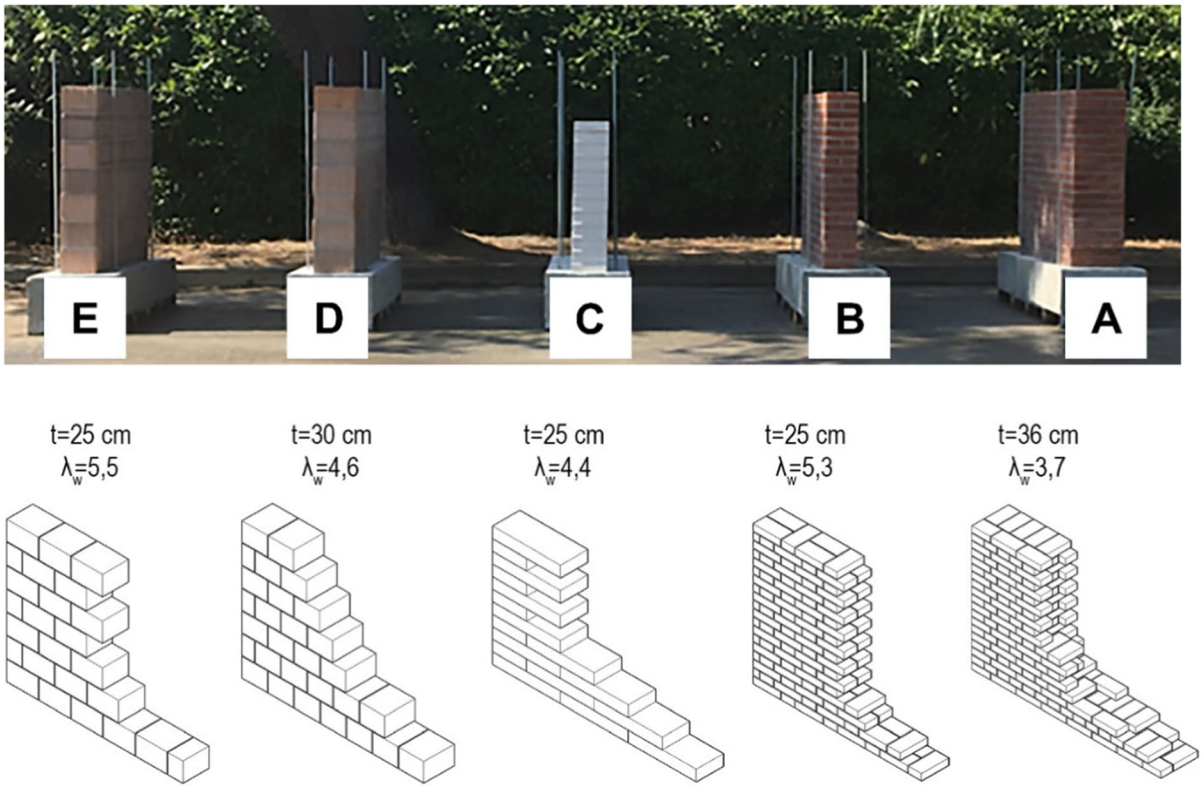

Fig. 1 Tested walls with indication of thickness t and slenderness ratio λ_w (height/thickness)

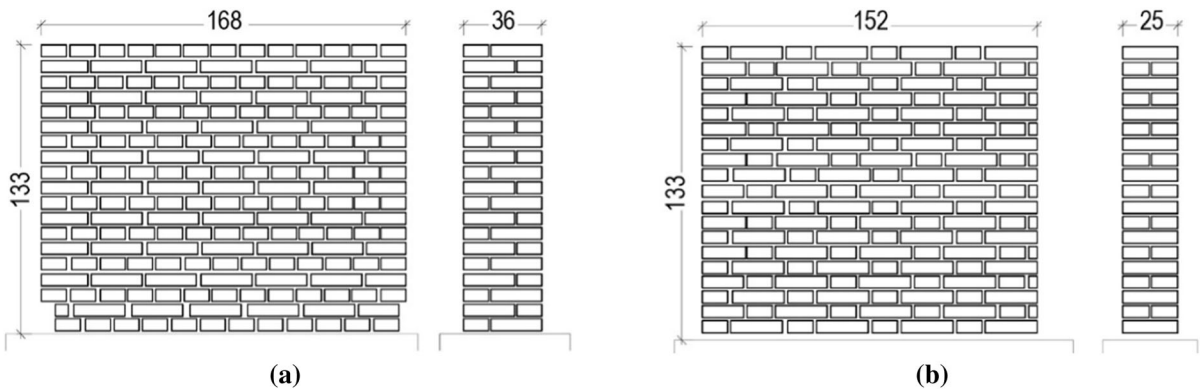

Fig. 2 Geometric features and masonry texture of wall A (**a**) and wall B (**b**)—units in cm

procedure are listed in Table 1. Afterwards, 8 specimens of mortar joints were tested in laboratory to measure the compressive and flexural strength according to UNI EN 1015-11:2007 [46]: first a bending test is performed. Then, compressive tests are carried out on the two parts of the original specimens (named compression (1) and compression (2) in Table 2) broken in the bending tests. Once that the mechanical properties of the mortar joints are known, and those of the units are provided by the manufacturer (Table 3), the characteristic compressive strength f_k can be calculated according to the expression given in Eurocode 6 [47]:

$$f_k = k \cdot f_b^{0.7} \cdot f_m^{0.3}, \quad (1)$$

Table 1 Mean mechanical parameters of mortar joints tested in situ with PNT-G tests (f_m mortar compressive strength)

	A	B	C	D	E
$f_{m,min}$ (MPa)	8.1	6.6	4.8	8.1	4.2
$f_{m,max}$ (MPa)	13	9.6	5.8	12.9	4.6
$f_{m,mean}$ (MPa)	10.6	8.1	5.3	10.5	4.4

where f_b is the units average compressive strength in MPa, f_m is the mortar compressive strength in MPa and k is a constant equal to 0.55 for full clay brick and AAC masonry and 0.45 for perforated clay brick masonry. The obtained values are $f_k = 20$ MPa and 18.5 MPa (wall A and B), 2.6 MPa (wall C), 7.9 MPa and 6.1 MPa (wall D and E). For a direct comparison with values indicated by the Italian Standards for existing masonry buildings [48], the mechanical parameters reported in Table 3 confirm the correct range suggested for perforated clay units masonry, being the values for walls D and E between 1.0 and 8.0 MPa. A comparison for walls A and B cannot be made since the Italian Standards indicate the values only for full clay units masonry with lime mortar, and not for cementitious mortar. However, the values found for the compressive strength are at least four times greater than those indicated for lime mortar and full clay units masonry (Table 3).

2.2 Testing procedures

The testing procedure consisted in performing pull-out tests on 108 strength anchors installed in different positions of the walls. The following phases were executed for the anchors installation: (1) hole drilling; (2) cleaning of the holes; (3) injection of resins with a filling height in the range of 50% and 75% of h (embedment depth); (4) bar installation. Perforation (1) was made by simple drilling percussion, this in order to reduce the vibration in holed bricks. Step (2) was performed first with pipe cleaner and after with

Table 2 Mean mechanical parameters of mortar joints tested in laboratory according to UNI EN 1015-11:2007 ($f_{c,mean}$ mean compressive strength, $f_{f,mean}$ mean flexural strength)

	Walls A–B–D–E		Wall C	
	Compression (1)	Compression (2)	Compression (1)	Compression (2)
$f_{c,mean}$ (MPa)	4.98	5.16	13.95	13.83
$f_{f,mean}$ (MPa)	8.7		17.6	

Table 3 Average characteristics of materials

Material	Young modulus (MPa)	Shear modulus (MPa)	Specific weight (kN/m^3)	Compressive strength (MPa)	Tensile strength (MPa)
Clay brick	n.a.	n.a.	19.1	62	n.a.
Autoclaved aerated concrete	n.a.	n.a.	5.5	4.4	n.a.
Perforated units	n.a.	n.a.	11.1	22	n.a.
Steel cl. 8.8 [49]	210,000	70,000	78	–	640
Concrete C30/35	30,000	13,600	25	–	1000
Masonry (full clay brick and lime mortar) [48]	1200–1800	400–600	18	2.6–4.3	$\cong$ 0
Masonry (perforated clay brick and cement based mortar) [48]	3500–5600	875–1400	15	5.0–8.0	$\cong$ 0
Epoxy resin (UNI EN 196-1:2016)	3700	10.5	16.2	–	80

n.a.—not experimentally determined

compressed air. The cleaning of the holes is essential remove in order to guarantee the best adhesion interface. The installation of the anchors, all of 10 mm diameter, was realized with a combination of injection and rotation in order to guarantee a better distribution of resin in the holes. For full brick walls (A, B, C) the hole diameter is 12 mm, whereas for walls with perforated (or hollow) units (D and E) the hole diameter is 16 mm. To avoid material dispersion in D and E walls, a proper steel sock was fitted in the wall before the adhesive injection.

Before testing, each wall was pre-compressed to simulate the effect of a slab acting on the masonry wall. The precompression was realized through two pairs of steel tie-rods, connected each other with an HEA140 profile of length 150 cm and steel S235 at the top of the wall (Fig. 3). The tie-rods were pre-stressed to reach an equivalent pre-compression stress at the top of all the walls of 0.20 MPa.

The strength anchors were installed according to a designed configuration, in order to limit mutual interference of failure modes during the tests. For example, given the layout of Fig. 4a, the sequence of testing is identified by progressive numbers. In particular, two adjacent anchors were not tested consequently, the testing started from the rows at the top of the wall towards the bottom skipping intermediate rows (Fig. 4a).

For A and B walls, three positions were considered: header (He), stretcher (St) and mortar joints (Mo). For these cases, test $1 + 3n$ was made on headers, $2 + 3n$ on stretchers and $3(1 + n)$ on mortar joints, with $n \in N$ (Fig. 4a). For D and E walls, the anchors were installed both in the middle of the units (B) and in the mortar (again vertical, horizontal and corner) joints. For wall C, due to its low mortar joint thickness, the anchors were installed only in the middle of the units.

The identification label for the 108 tested anchors is $X - Y - \# - I$ where the first letter (X) indicates the tested wall, the second one (Y) the position of the anchor, the third one the embedment depth (#) and the fourth one a progressive number (I).

The pull-out tests were performed with a portable dynamometer with maximum pull-out capacity of 20 kN, *Ercolino® hydrotester* (AT.ED.3), shown in (Fig. 4b). This device is a hydraulic instrument in control of displacement. Through the rotation of mechanical levers, a displacement is imposed to the head of the anchors and the corresponding pressure on a manometer is read. The pull-out capacity of each of the 108 tested anchors was therefore registered and results elaborated as explained in the following paragraph.

2.3 Experimental results

The pull-out strength (P_{max}) is normalized with respect to the tensile strength of the anchors. That represents the upper limit of the performance than can be demanded to a tensile anchor. The capacity of the threaded anchor P_s is:

$$P_s = \frac{\pi}{4}\phi^2 f_y, \tag{2}$$

where ϕ is the diameter of the anchor and f_y the yielding stress. The efficiency of the anchors can be expressed by the ratio η_s:

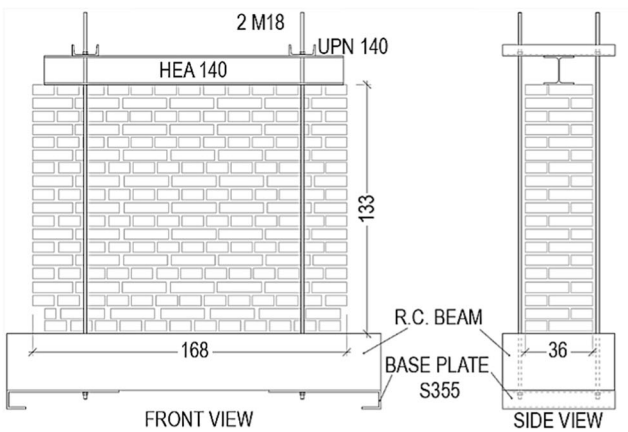

Fig. 3 Contrast system for the application of pre-stress on wall A through 2 + 2 steel bars—units in cm

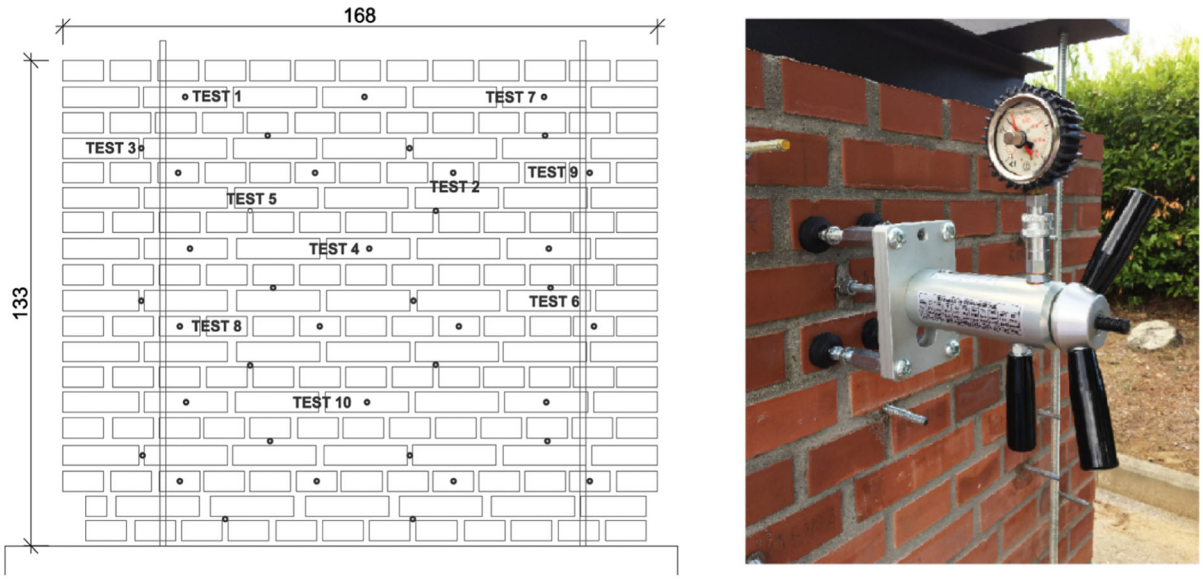

Fig. 4 Sequence of testing of wall A (units in cm) (**a**); Testing machine for the pull-out tests—*Ercolino® hydro-tester* (**b**)

$$\eta_s = \frac{P_{max}}{P_s}. \quad (3)$$

η_s can assume values in the range [0–1]: values closer to 1 indicate a greater anchor efficiency, whereas $\eta_s = 1$ means the failure of the steel bar.

Being wall type A and B made of clay brick with thickness of 36 cm and 25 cm respectively, the maximum relative depth is:

$$\frac{h_{max}}{t_{min}} = \frac{160}{250} = 64\%, \quad (4)$$

where h_{max} is the maximum depth of the anchors; t_{min} is the minimum thickness of the wall.

2.3.1 Walls A and B

The average pull-out strength of the anchors in brick units is 13.4 kN for wall A (thickness 36 cm) and 11.7 kN for wall B (thickness 25 cm). The average pull-out strength of the anchors in mortar joints is 11.4 kN for wall A (thickness 36 cm) and 13.6 kN for wall B (thickness 25 cm). The anchors in mortar joints have much greater pull-out strength ($P_{max,Mo}$) than those in bricks ($P_{max,bricks}$). Nevertheless, in half of the tests carried out for h = 120 mm and h = 160 mm the capacity of the *Ercolino hydrotester* (20 kN) is attained, but these values are excluded from the data elaboration for the sake of safety. Therefore, in Table 4 it appears that the ratio $P_{max,Mo}/P_{max,bricks}$ is close to 1 but it is actually much greater since the full-scale of the testing machine is reached in half of the tests. The maximum ratio of $P_{max,Mo}/P_{max,bricks}$, found for h = 120 mm, is 1.38 for B wall (Table 5). As for the variation of embedment depth, an increment of it by 80%—passing from 90 mm to 160 mm—leads to more than double of the pull-out strength for B wall

Table 4 Pull-out strength (P_{max}) of anchors, wall A

h (mm)	Header (kN)	Stretcher (kN)	Mortar (kN)	Mo J./brick (–)
90	11.2	11.2	11.4	1.02
120	13.8	10.1	10.4	0.87
160	17.0	17.1	16.4	0.96

Table 5 Pull-out strength (P_{max}) of anchors, wall B

h (mm)	Header (kN)	Stretcher (kN)	Mortar (kN)	Mo J./Brick (–)
90	5.3	7.9	8.5	1.29
120	11.6	9.3	14.4	1.38
160	17.0	19.2	18.0	0.99

(mortar joints 18.0/8.5 = 2.1 and bricks 19.2/7.9 = 2.4). The anchors in wall A do not exhibit the same significant increase: the corresponding ratios of P_{max} for anchors in mortar joints is 16.4/11.4 = 1.4 and for anchors in bricks 17.0/11.2 = 1.5.

The corresponding efficiency ratios are shown in Fig. 5, where the results are linearly interpolated. The best correlations—corresponding to greater correlation coefficients—are obtained for wall B for anchors in headers and in mortar joints (Fig. 5a, c). The corresponding efficiency ratio goes from 0.12 (h = 90 mm) to 0.35 (h = 160 mm), confirming the results of the literature according to which a greater embedment depth results in a greater normalized pull-out capacity [2].

Concerning the types of failures observed in the experimental campaign, the following modes can be identified:

- *SF* sliding failure;
- *BPF* brick pull-out failure;
- *BCF* brick-cone failure;
- *MBIF* mortar brick interface failure.

It is worthy to notice that the distance from the anchor to the reaction points of the device, being about 15 cm, could interfere with the formation of possible brick-cone failures, although this type of failure is generally rare for anchors in masonry. The most common failure mode of anchors in walls A and B is the sliding failure (Fig. 6a) respectively 72% and 60% of the total failure modes, as listed in Table 6.

This result is valid for both the anchors placed in bricks and for those placed in mortar joints. The percentage of SF is less for the anchors placed in the mortar joint, for which the number of mortar brick interface failures (MBIF) is not negligible. The number of brick pull-out failures is very small, but still present (Fig. 6b).

As already mentioned, a significant percentage of failure is classified as Full Scale Failure (FSF). The percentage of FSF is basically found more for anchors in mortar joints than in bricks, due to their greater strength value. Indeed, the shear strength of mortar joints is significantly larger than that of bricks.

2.3.2 *Walls C, D and E*

The tests on wall C gave pull out strength values too small and too scattered to be significantly analysed. Moreover, for walls D and E (made of vertically perforated units with voids percentage lower than 36%), the pull-out average capacity is about 7 kN for anchors in bricks (almost half of th of wall A). The average pull-out strength for anchors in mortar joints is similar to the minimum observed for walls A and B (about 10 kN).

The pull-out strength in anchors in mortar joints becomes significantly greater than that in bricks for high embedment depths (Table 7). Moreover, the pull-out capacity for anchors in bricks slightly decreased by increasing the injection depth. This trend is the opposite with respect to what observed for masonry made of bricks without voids.

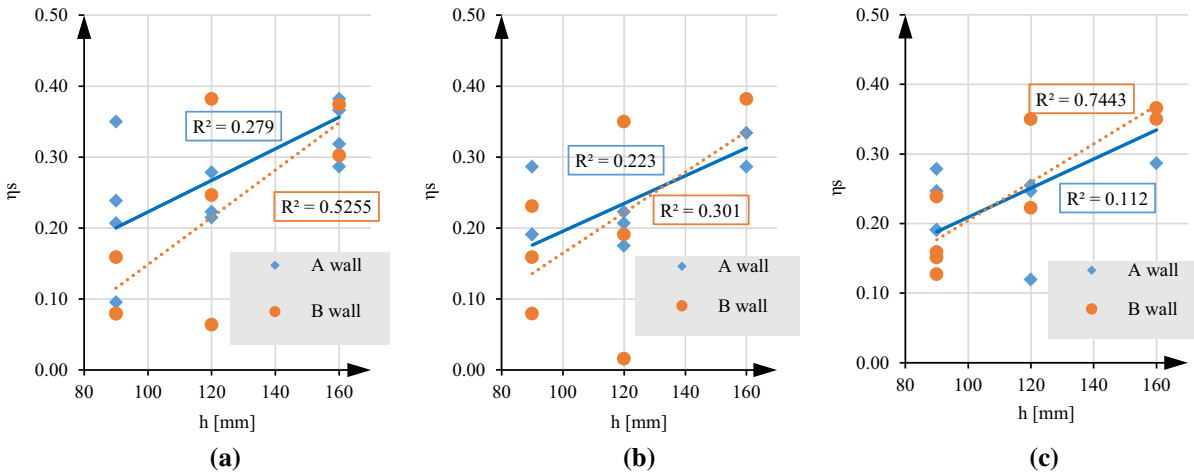

Fig. 5 Efficiency of the anchors installed in walls A and B, in headers (**a**); stretchers (**b**); mortar joints (**c**)

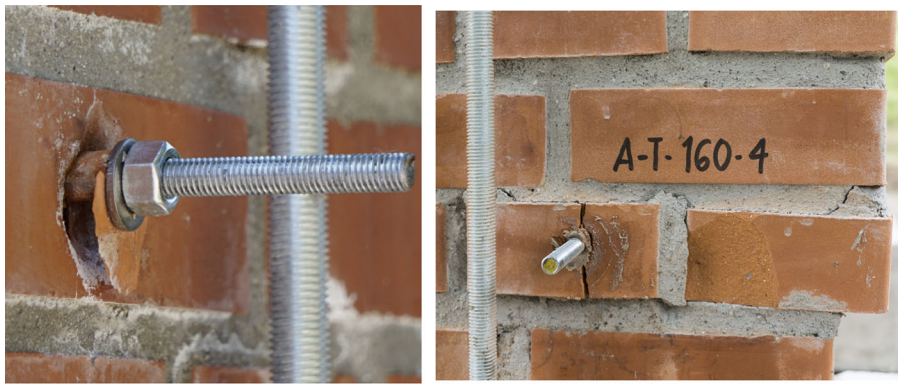

Fig. 6 Sliding failure (**a**) and brick pull-out failure (**b**)

Table 6 Distribution of the failure modes for walls A and B

Failure mode	Wall A			Wall B		
	Brick	Mortar joint	Total	Brick	Mortar joint	Total
SF	90%	50%	72%	78%	42%	60%
BCF	–	–	–	5%	–	3%
BPUF	5%	–	2%	–	–	3%
MBIF	–	11%	5%	–	25%	13%
FSF	5%	39%	21%	17%	33%	21%

Table 7 Pull-out strength (P_{max}) of anchors, walls D and E

	h (mm)	Bricks (kN)	Mortar (kN)	Mo J./Brick (kN)
D	90	9.0	9.3	1.03
	160	4.8	7.7	1.61
E	90	9.9	10.4	1.05
	160	4.4	12.4	2.82

Table 8 reports the failure modes observed for walls D and E: in this case, the predominant failure mode is SF followed by the SF combined with BCF (Fig. 7), therefore a mixed type failure as often occurs for anchors in masonry [33]. Due to the difficulties in discerning the failure types and to the poor number of tests successfully finalized, these results are excluded from an analytical interpretation.

Table 8 Distribution of the failure modes for walls E and D

Failure mode	Wall D			Wall E		
	Brick	Mortar Joint	Total	Brick	Mortar Joint	Total
SF	100%*	88%	91%*	100%**	100%**	100%**
BPF	–	–	–	–	–	–
BCF	–	22%	9%	–	–	–

*Combined failure SF + BPF

**Combined failure SF + BCF

(a) (b)

Fig. 7 Combined sliding failure and block cone failure (**a**) and combined sliding failure and block failure (**b**)

3 Analytical interpretation

This section contains an analytical interpretation of the experimental tests with the proposal of design indications. Firstly, a brief description of the existing analytical models, available in the literature mainly for strength anchors embedded in concrete elements, is given. Then, the comparison is performed by fitting the analytical predictions with the experimental results. Finally, an original analytical model is proposed to obtain information about the failure mode of the strength anchor, depending on the material mechanical and geometric characteristics.

3.1 Existing analytical models

As already reported in the Introduction, the analytical models available in the literature are mainly referred to the anchors pull-out capacity in concrete specimens (Table 9). Some of them are based on the plasticity theory (model 1 or uniform stress model, 3, 4 in Table 9).

Model 3 (concrete cone model) only depends on the embedment length and the compressive strength of the surrounding concrete. Model 4 is the combined cone-bond stress model where the anchor capacity is found superposing the pull-out resistance of the cone and the bond. The first two models deal with a pure sliding failure. In the interpretation of the experimental tests, models 1 and 2 are considered, since most tests exhibited sliding failures,. The bond stress is frequently considered to have uniform distribution along the anchor length. This hypothesis is only valid for short embedment depths whilst the uniform stress model overestimates the anchor capacity for longer depths [39]. In particular, as also stated in [17], the uniform stress model and the elastic bond stress model (model 2) give similar results for embedment depths up to $40\sqrt{\varphi_0}$(φ_0 is the hole diameter). The maximum embedment depths of the anchors used in the experimental campaign is 160 mm and therefore, since 120 mm $< 40\sqrt{12} = 139$ mm, the hypothesis of uniform stress is acceptable for the embedment depths of 90 mm and 120 mm.

Table 9 Main analytical models for the estimation of the pull-out strength of anchors in concrete

Model	Pull out strength	References
1	$P_{max} = \tau_0 \pi \phi_0 h_{ef}$	Mc Vay et al. [35]
2	$P_{\max} = \tau_{\max} \pi \phi_0 \left(\frac{\phi_0^{0.5}}{\lambda'} \tan h \left(\frac{\lambda' h_{\mathrm{ef}}}{\sqrt{\phi_0}} \right) \right)$	Doerr and Klingner [39] Cook et al. [36]
3	$P_{max} = 0.85 h_{ef}^2 \sqrt{f_{ck}}$	Eligehausen et al. [37]
4	$P_{\max} = 0.85 h_{\mathrm{c}}^2 \sqrt{f_{\mathrm{ck}}} + \tau_0 \pi \phi_0 (h_{\mathrm{ef}} - h_{\mathrm{c}})$	Cook et al. [15, 36]
5	$P_{\max} = \frac{\alpha \tau_{\max}}{k} (E_{\mathrm{s}} A_{\mathrm{s}} \cosh \alpha h_{\mathrm{ef}})$	Froli [38]

3.2 Comparison of experimental results with literature models

3.2.1 Model 1

The uniform stress model is associated to the SF (sliding failure), that is the shear breaking of the interface between resin and brick. According to this model, the pull-out capacity is [35] (Table 9):

$$P_{\max} = \pi \tau_0 \phi_0 h_{\text{ef}}. \tag{5}$$

Equation (5) is here used to calculate the shear stress at the interface ($\tau_{0,i}$) relative to the pull-out value $P_{\max,i}$ of the tested anchors. The results are shown in Fig. 8a and represent the normal distribution of the experimental value ($\tau_{0,i}$). The blue line of Fig. 8b represents model 1 and matches closely the red dashed linear interpolant for the experimental data. Therefore, this model can be advantageously used in order to calculate the pull-out capacity also for anchors in masonry.

The use of Eq. (5) where τ_0 is unknown and the other parameters are available from the experimental tests provides a uniform tangential stress of τ_0 = 2.8 MPa. This experimental shear stress is about 35 times greater than the one provided by the Italian standards for a similar masonry, although with lime mortar [48]. This effect can be attributed to (1) a local consolidation effect given from the epoxy resin; (2) a local better behaviour of masonry with respect to the average value used in the global verification.

3.2.2 Model 2

The model proposed by Doerr and Cook [15, 17, 39] is based on the elastic distribution of the tangential stress. The failure occurs when the maximum shear stress at the interface between resin and masonry is obtained. The expression provided for the pull-out capacity is:

$$P_{\max} = \frac{\pi}{\lambda'} \tau_{\max} \phi_0^{\frac{3}{2}} \left(\tan h \left(\frac{\lambda' h_{\text{ef}}}{\sqrt{\phi_0}} \right) \right), \tag{6}$$

where λ' is a coefficient which accounts for the characteristics of the resin and of the epoxy bar and is expressed by

$$\lambda' = \sqrt{\frac{4G_{\text{er}}}{tE}}. \tag{7}$$

Considering the shear modulus G_{er}= 10.5 MPa (epoxy resin, Table 3) the value of this coefficient is λ' = 0.014. Taking the average value from experimental data, a value of $\tau_{\max}$ = 3.0 MPa is obtained, which is about 7% more than the average value τ_0 found for model 1. Also in this case, the equation proposed is in good agreement with the experimental data (Fig. 9). Again, the obtained average shear tension is one order of magnitude greater than that indicated by the Italian standards [48].

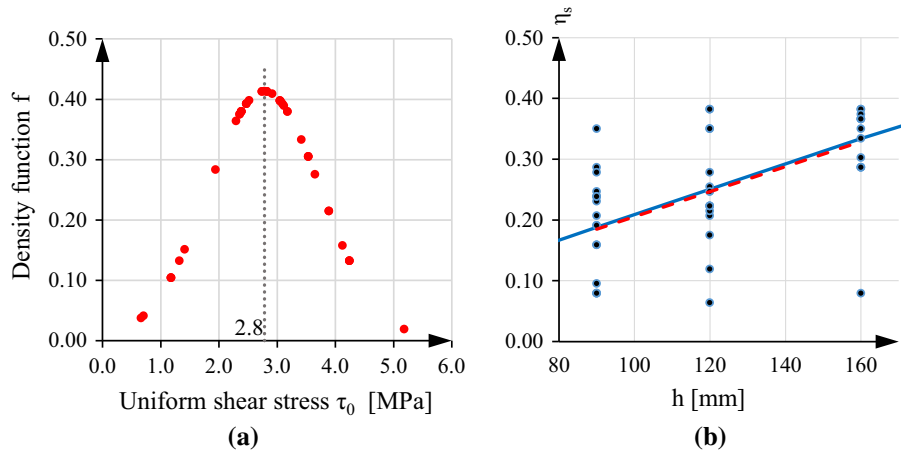

Fig. 8 Normal distribution of the shear stress value $\tau_{0,i}$ of wall A and B (**a**); linear interpolation of the experimental data (**b**) with model 1, where the red dashed line is the linear interpolation of the experimental data, and the blue solid line represents model 1

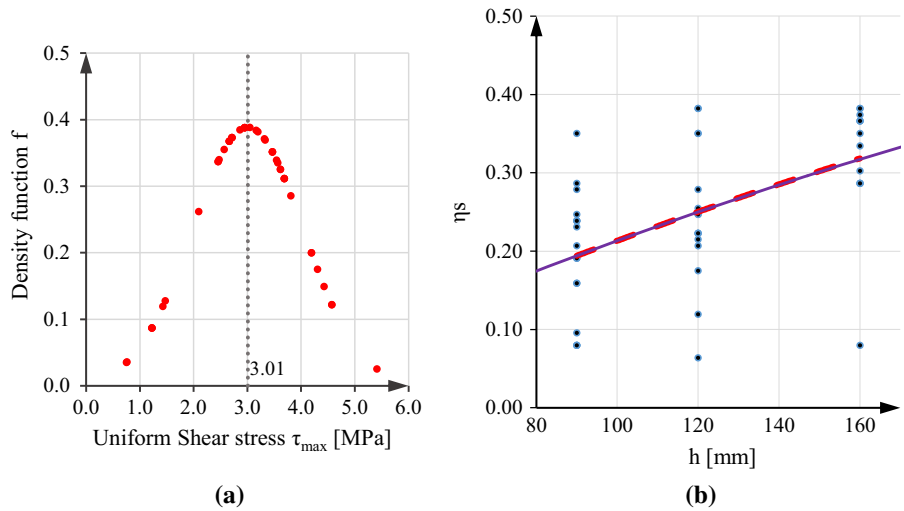

Fig. 9 Normal distribution of the stress value τ_{max} of wall A and B (**a**); parabolic interpolation of the experimental data (**b**) with model 2, where the red dashed line is the parabolic interpolation of the experimental data and the violet solid curve represents model 2

3.3 Proposed analytical model and design indications

The masonry wall is considered as an elastic homogeneous solid defined by the mechanical constants (E, v, G) subjected to an axial load along z axis (Fig. 10). The threated anchor is considered as a monoaxial element of finite stiffness completely embedded in the masonry solid.

The problem presents a geometric axial symmetry and a free edge. Considering a masonry cylinder of radius r_m surrounding a steel anchor of radius r_s, from the equilibrium one has that the shear stress on masonry τ_m is:

$$\tau_m = f(r_m) = \frac{\tau_s r_s}{r_m}. \tag{8}$$

Equation (8) describes the trend of τ_m increasing the radius r_m and clearly shows that τ_m decreases with a hyperbolic law.

For an elastic material the shear deformation is:

$$\varepsilon_{zr} = \frac{\tau_{zr}}{2G_m}, \tag{9}$$

in which G_m is the masonry shear modulus.

Considering that $P = 2\pi\tau_s r_s h_{ef}$ and substituting Eq. (8) in Eq. (9) the shear deformation becomes:

$$\varepsilon_{zr} = \frac{1}{r_m}\frac{P}{4\pi h_{ef} G_m}. \tag{10}$$

The axial displacement from r_s to a generic value r_m is:

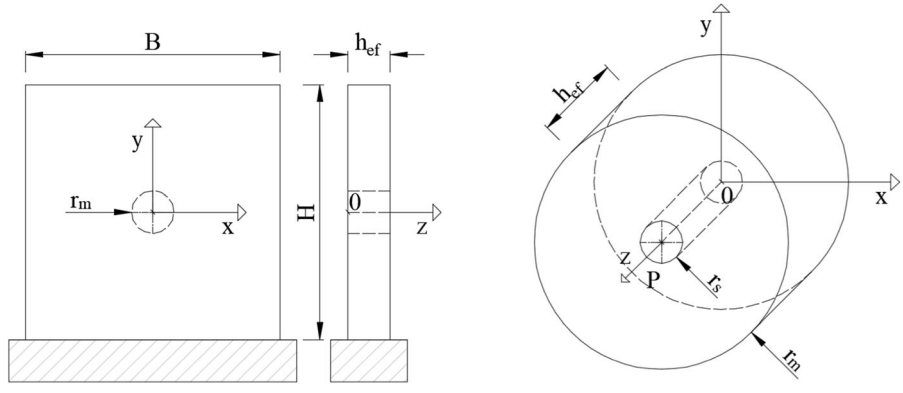

Fig. 10 Schematics of the generic masonry panel with $h_{ef} = t$

$$\delta = \int_{r_s}^{r_m} \varepsilon_{zr} dr = \int_{r_s}^{r_m} \frac{1}{r} \frac{P}{4\pi h_{ef} G_m} dr, \quad (11)$$

where r is the generic radius of the masonry cylinder, then the elastic displacement of the masonry part is:

$$\delta = \frac{P}{4\pi h_{ef} G_m} \log\left(\frac{r_m}{r_s}\right). \quad (12)$$

The elastic displacement of the threaded bar is:

$$\delta_s = \frac{P h_{ef}}{2 E_s A_s}. \quad (13)$$

So it is possible to calculate the distance r_m such that the ratio δ/δ_s becomes less than a selected threshold value ψ. This consideration is made in order to limit the elastic displacement of masonry to avoid undesired brittle failure:

$$\frac{\delta}{\delta_s} \leq \psi. \quad (14)$$

Including Eqs. (12) and (13) in (14) one has:

$$r_m \leq r_s \cdot 10^{\frac{2\psi G_m h_{ef}^2}{E r_s^2}}. \quad (15)$$

From which:

$$\frac{r_m}{r_s} = 10^{\frac{2\psi G h_{ef}^2}{E r_s^2}}. \quad (16)$$

Equation (16) is plotted in Fig. 11 considering the variation of the shear modulus G_m and different values of ψ. A radius of the anchor of 5 mm is considered.

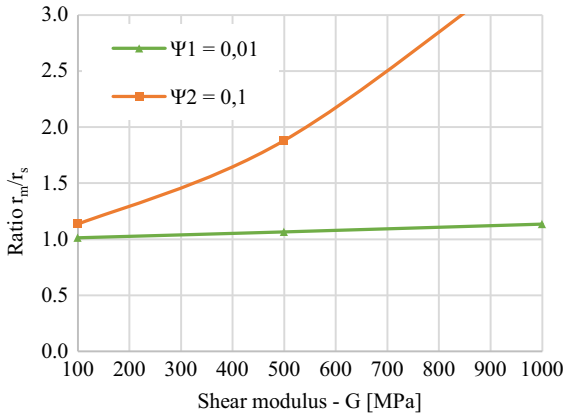

Fig. 11 Ratio r_m/r_s versus masonry shear modulus (h_{ef} = 120 mm)

For threshold values of ψ included between 0.01 and 0.1, the masonry radius normalized to the steel anchor radius significantly changes. In particular, when the masonry failure displacement is assumed very low with respect to that of steel, the masonry cylinder roughly coincides with the anchor itself ($r_m \cong r_s$) independently from the masonry shear modulus.

For an intermediate value of ψ = 5% and for moderate embedment depths (up to 25 times the normalized depth h_{ef}/r_s), the radius of masonry is very similar to that of the steel anchor (Fig. 12), independently from the material properties. This is usually the case of anchors injected in masonry for which, as observed in the experimental tests, the most recurring failure mode is the splitting failure. For greater embedment depths, the masonry cylinder involved in the failure exponentially increases especially for strong masonry (G = 800, 1000 MPa). Considering a clay brick masonry with lime mortar, G = 400–600 MPa), whereas for a clay brick masonry with cementitious mortar this value increases to 900–1400 MPa [48].

For short anchors, as those tested in the experimental campaign, the analytical model and the experimental tests showed that the masonry portion involved in the failure is very limited and therefore the most likely failure type is sliding failure. Confirming the results found in the literature, for short anchors (up to $40\sqrt{\varphi_0}$), the uniform bond stress model

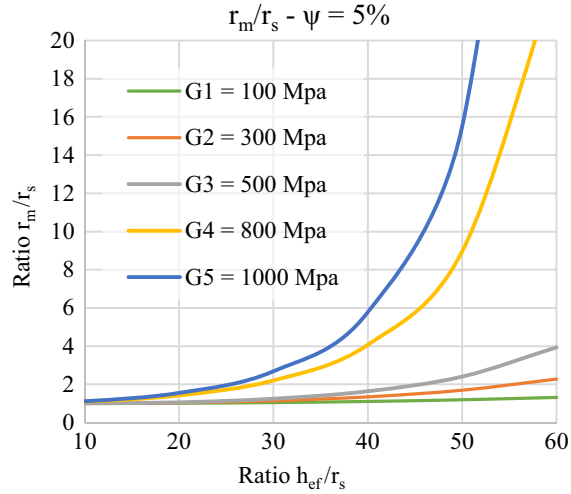

Fig. 12 Ratio r_m/r_s versus normalized depth h_{ef}/r_s

is able to predict a reliable value of the pull-out strength.

4 Conclusions

The experimental tests illustrated in this paper allowed broadening the knowledge about the beahviour of anchors injected in full clay brick masonry and in hollow block masonry.

For masonry specimens of **full clay bricks**, the results revealed that the chemical **anchors injected in mortar joints** have much greater pull-out strength than that found for anchors injected in bricks. As for the variation of **embedment depth**, an increment of it by 80%—passing from 90 mm to 160 mm—causes an increase of pull-out strength by minimum 40% (and up to 270%).

The corresponding efficiency ratio (between experimental pull-out resistance and tensile strength of the anchor) goes from 0.12 (h = 90 mm) to 0.35 (h = 160 mm).

As for the **hollow block masonry**, the pull-out strength for anchors in bricks decreases by increasing the injection depth. This trend is the opposite with respect to what observed for masonry made of full bricks, as expected since in full bricks the failure surface is greater. For hollow brick masonry the pull-out strength in anchors injected mortar joints becomes significantly greater than that in blocks for high embedment depths.

The most common **failure mode** is the sliding failure, followed by the mortar brick interface failures (for full clay brick masonry) and by a sliding failure combined with block failure (for hollow block masonry).

An analytical model is proposed for defining the masonry solid surrounding the anchor which participates to failure. The model proposed considers an anchor in a generic elastic half-space and it allows (1) to keep the elastic displacement of the masonry portion under a threshold value to avoid or at least to limit brittle failures and (2) to identify the best model to use among those available in the literature. Indeed, sliding failure occurred for short anchors or weak masonry and mixed sliding/cone failure occurred for long anchors or strong masonry.

Consequently, the uniform stress model can be successfully used to predict pull-out strength values of anchors installed in masonry walls with characteristics similar to those of the walls tested.

Acknowledgements Open access funding provided by Università di Pisa within the CRUI-CARE Agreement. The authors wish to thank the sponsorship of the Italian Department of Civil Protection, in the framework of the RELUIS Project - Masonry Structures (2019), the company LIVITH SPA (Montespertoli, Florence) and particularly Dr. Giacomo di Furia for its financial support in performing the experimental tests. The authors also thank Eng. Erika Doveri for collecting data from experimental tests.

Compliance with ethical standards

Conflict of interest The authors declare that they have no conflict of interest.

References

1. Proença JM, Gago AS, Boas AV (2019) Structural window frame for in-plane seismic strengthening of masonry wall buildings. Int J Archit Herit 13(1):98–113
2. Müsevitoğlu A, Arslan MH, Aksoylu C, Özkış A (2020) Experimental and analytical investigation of chemical anchors's behaviour under axial tensile. Measurement 158:107689
3. Karáseka R, Bajer M, Jurdová K (2012) Influence of column construction type on the bearing capacity of bonded anchors. Proc Eng 40:195–198
4. Muñoz R, Lourenço PB (2019) Mechanical behaviour of metal anchors in historic brick masonry: an experimental approach. In: Structural analysis of historical constructions, Springer International Publishing, pp 788–798. https://doi.org/10.1007/978-3-319-99441-3_85
5. Paganoni S, D'Ayala D (2014) Testing and design procedure for corner connections of masonry heritage buildings strengthened by metallic grouted anchors. Eng Struct 70:278–293
6. Alecci V, De Stefano M, Luciano R, Marra A, Stipo G (2020) Numerical investigation on the use of flat-jack test for detecting masonry deformability. J Test Eval 49. https://doi.org/10.1520/JTE20190781

7. Casapulla C, Jossa P, Maione A (2010) Rocking motion of a masonry rigid block under seismic actions: a new strategy based on the progressive correction of the resonance response. Ing Sismica 27(4):35–48
8. Casapulla C (2015) On the resonance conditions of rigid rocking blocks. Int J Eng Technol 7(2):760–771
9. Solarino F, Oliveira D, Giresini L (2019) Wall-to-horizontal diaphragm connections in historical buildings: a state-of-the-art review. Eng Struct 199:109559
10. Giresini L (2017) Design strategy for the rocking stability of horizontally restrained masonry walls. In: COMPDYN 2017 6th ECCOMAS thematic conference on computational methods in structural dynamics and earthquake engineering
11. Giresini L, Solarino F, Paganelli O, Oliveira DV, Froli M (2019) One-sided rocking analysis of corner mechanisms in masonry structures: influence of geometry, energy dissipation, boundary conditions. Soil Dyn Earthq Eng 123:357–370
12. Giresini L, Sassu M, Sorrentino L (2018) In situ free-vibration tests on unrestrained and restrained rocking masonry walls. Earthq Eng Struct Dyn 47(15):3006–3025
13. AA.VV (2011) ETAG001—metal anchors for use in concrete
14. AA.VV (2013) ETAG—metal Injection anchors for use in masonry, no. December 1988
15. Eligehausen R, Cook RA, Appl J (2006) Behavior and design of adhesive bonded anchors. ACI Struct J 103(6):822–831
16. Zamora N, Cook R, Konz R (2003) Behavior and design of single, headed and unheaded grouted anchors under tensile load. ACI Struct J 100(2):222–230
17. Subramanian N, Cook RA (2002) Installation, behaviour and design of bonded anchors. Indian Concr J 76(1):47–56
18. Sakla SSS, Ashour AF (2005) Prediction of tensile capacity of single adhesive anchors using neural networks. Comput Struct 83(21):1792–1803
19. Ozturk M (2013) Prediction of tensile capacity of adhesive anchors including edge and group effects using neural networks. Sci Eng Compos Mater 20(1):95–104
20. Dizhur D, Schultz A, Ingham J (2016) Pull-out behavior of adhesive connections in unreinforced masonry walls. Earthq Spectra 32(4):2357–2375
21. Arifpovic F, Nielsen MP (2006) Strength of anchors in masonry. Department of Civil Engineering, Technical University of Denmark, Rapport BYG DTU, ISBN 87-7877-205-2
22. Alecci V, Stipo G, La Brusco A, De Stefano M, Rovero L (2019) Estimating elastic modulus of tuff and brick masonry: a comparison between on-site and laboratory tests. Constr Build Mater 204:828–838
23. Alecci V, Fagone M, Rotunno T, De Stefano M (2013) Shear strength of brick masonry walls assembled with different types of mortar. Constr Build Mater 40:1038–1045
24. Sassu M, Giresini L, Bonannini E, Puppio ML (2016) On the use of vibro-compressed units with bio-natural aggregate. Buildings 6(3):40
25. Casapulla C, Maione A (2018) Experimental and analytical investigation on the corner failure in masonry buildings: interaction between rocking-sliding and horizontal flexure. Int J Archit Herit Conserv Anal Restor 14(2):208–220
26. Sassu M, Andreini M, Casapulla C, De Falco A (2013) Archaeological consolidation of UNESCO masonry structures in Oman: the sumhuram citadel of Khor Rori and the Al Balid Fortress. Int J Archit Herit 7(4):339–374
27. Casapulla C, Cascini L, Portioli F, Landolfo R (2014) 3D macro and micro-block models for limit analysis of out-of-plane loaded masonry walls with non-associative Coulomb friction. Meccanica 49(7):1653–1678
28. Sassu M (2006) The reinforced cut wall (RCW): a low-cost base dissipator for masonry buildings. Earthq Spectra 22(2):533–554
29. Alecci V, De Stefano M (2019) Building irregularity issues and architectural design in seismic areas. Frat Integr Strut 13(57):161–168
30. Alecci V, De Stefano M, Galassi S, Lapi M, Orlando M (2020) An Assessment of American Criterion for Detecting Plan Irregularity. In: Köber D, Stefano M, Zembaty Z (eds) Seismic behaviour and design of irregular and complex civil structures Geotechnical, Geological and Earthquake Engineering, vol 48
31. Mistretta F, Stochino F, Sassu M (2019) Structural and thermal retrofitting of masonry walls: an integrated cost-analysis approach for the Italian context. Build Environ 155:127–136
32. Sassu M, Stochino F, Mistretta F (2017) Assessment method for combine structural and energy retrofitting in masonry buildings. Buildings 7:71
33. Ceroni F, Di Ludovico M (2020) Traditional and innovative systems for injected anchors in masonry elements: experimental behavior and theoretical formulations. Constr Build Mater 254:119178
34. Moreira S, Ramos LF, Oliveira DV, Lourenço PB (2014) Experimental behavior of masonry wall-to-timber elements connections strengthened with injection anchors. Eng Struct 81:98–109
35. McVay M, Cook RA, Krishnamurthy K (1983) Pullout simulation of postinstalled chemically bonded anchors. J Struct Eng 122(9):1016–1024
36. Cook RA, Doerr GT, Klingner RE (1993) Bond stress model for design adhesive anchors. ACI Struct J 90:514–524
37. Eligehausen R, Mallée R, Rehm G (1985) Befestigungen mit Verbundankern. Betomverk + Fertigteil Technik 10:686–692
38. Froli M (2007) Analytical remarks on the anchorage of elastic–plastically bonded ductile bars. Int J Mech Sci 49(5):589–596
39. Doer GT, Klingner RE (1989) Adhesive anchors: behaviour and spacing requirements
40. Fuchs W, Eligehausen R, Breen JE (1995) Concrete capacity design (CCD) approach for fastening to concrete. Struct J 92(1):73–94
41. Sasmal S, Thiyagarajan R, Lieberum KH, Koenders EAB (2018) Numerical simulations of progression of damage in concrete embedded chemical anchors. Comput Concr 22(4):395–405
42. Ceroni F, Darban H, Luciano R (2020) Analysis of bond behavior of injected anchors in masonry elements by means of Finite Element Modeling. Compos Struct 241:112099
43. Gigla B, Wenzel F (2012) Design recommendations for injection anchors as supplementary reinforcement of

historic masonry. In: Proc. 12th International brick/block masonry conference, Madrid, Spain, pp 691–706
44. Gigla B (2012) Structural design of supplementary injection anchors inside masonry. In: 15th international brick and block masonry conference, Florianópolis—Brazil
45. Gucci N, Barsotti R (1995) A non-destructive technique for the determination of mortar load capacity in situ. Mater Struct 28:276–283
46. UNI EN 1015:11 2017 Methods of test for mortar for masonry—Part 11: determination of flexural and compressive strength of hardened mortar
47. Eurocode 6: Design of masonry structures—part 1-1: General rules for reinforced and unreinforced masonry structures. The European Union Per Regulation 305/2011, Directive 98/34/EC, Directive 2004/18/EC
48. Ministero delle infrastrutture e dei trasporti (2019) Circolare 21 gennaio 2019, n. 7 Istruzioni per l'applicazione dell' « Aggiornamento delle "Norme tecniche per le costruzioni"», pp 1–337
49. Decreto Ministeriale 17/01/2018, Italian Technical Standards for buildings (Nuove Norme Tecniche per le Costruzioni, in italian) (2018)
50. General Assembly of the Superior Council of Public, Circolare attuativa del D.M. 17/01/2018 (NTC 2018) (2019)